Chemical Geology 332–333 (2012) 102–115

Contents lists available at SciVerse ScienceDirect

Chemical Geology

journal homepage: www.elsevier.com/locate/chemgeo

Relative retention of trace element and oxygen isotope ratios in zircon from Archean rhyolite, Panorama Formation, North Pole Dome, Pilbara Craton, Western Australia

Kouki Kitajima [a,*], Takayuki Ushikubo [a], Noriko T. Kita [a], Shigenori Maruyama [b], John W. Valley [a]

[a] WiscSIMS Laboratory, Department of Geoscience, University of Wisconsin, 1215 W. Dayton St., Madison, WI 53706, USA
[b] Department of Earth and Planetary Sciences, Tokyo Institute of Technology, 2-12-1 Ookayama, Meguro, Tokyo 152–8551, Japan

ARTICLE INFO

Article history:
Received 30 March 2012
Received in revised form 9 September 2012
Accepted 10 September 2012
Available online 18 September 2012

Editor: K. Mezger

Keywords:
Zircon
Oxygen isotope ratio
Trace elements
SIMS
Archean
Pilbara craton

ABSTRACT

In-situ analyses for oxygen isotope ratio and trace element concentration by ion microprobe of 3.3–3.7 Ga zircons from rhyolite of Panorama Formation in the North Pole Dome, Pilbara Craton document intracrystalline patterns of variability, show compositional correlation, and provide metrics to assess alteration.

Values of $\delta^{18}O$ in the North Pole Dome (NPD) zircons average 5.78 ‰ with a tight range from 5.3 to 6.4 ‰ VSMOW. These values are similar to magmatic zircons throughout the Archean worldwide and there is no correlation of $\delta^{18}O$, U–Pb age, or trace elements. SEM/CL examination shows no evidence of mineral inclusions in the SIMS analysis pits. *In-situ* analysis of Ca concentration is useful to assess the degree of alteration in zircon and retention of trace element compositions. Most zircon analyses (74 %) have elevated [Ca] ≥ 120 ppm, with values up to 1614 ppm suggesting alteration, probably facilitated by radiation damage. Many high-Ca zircons show enrichment in middle–heavy REE (M–HREE), a peak near Dy, and concave-down trends in chondrite-normalized diagrams. The calculated Dy anomalies (Dy/Dy*) correlate with [Ca]. High Ca also correlates with P, Ti, Fe, Y and REE, and with cumulative (unannealed) α-doses from radiactive decay of Th and U (3.1 to 20×10^{15} events/mg). If not annealed, this α-dose could have caused radiation damage that exceeded the first percolation point. Radiation damage can also facilitate alteration of $\delta^{18}O$ in zircon, but examples from other terranes show that alteration is heterogeneous and correlates to greater variability of $\delta^{18}O$ within and among zircons. The tight range of oxygen isotope ratios in the NPD rhyolite zircons and their similarity to other Archean zircons, world-wide, suggests that the analyzed NPD zircons have retained original, magmatic oxygen isotope ratios.

© 2012 Elsevier B.V. All rights reserved.

1. Introduction

Zircon is a common accessory mineral in a wide range of mafic to felsic igneous rocks, and can preserve a record of magmatic geochronology and geochemistry. Because of its resistance to physical and chemical alteration, Archean zircons, even detrital or xenocrystic grains, are used to estimate age (U–Pb), oxygen isotope ratio, and trace element composition of parental magmas (Hoskin and Schaltegger, 2003; Ireland and Williams, 2003; Parrish and Noble, 2003; Valley, 2003; Valley et al., 2005). Zircons, however, are susceptible to radiation damage and alteration that can selectively affect specific U- and Th-rich domains within a single crystal. Different geochemical systems can be affected under different conditions, especially for comparison of major (e.g., oxygen) vs. trace elements. *In-situ* analysis documents intracrystalline patterns of variability, allowing correlation of compositions, and provides metrics to assess alteration.

Zircon alteration is especially likely if radiation damage accumulates due to high Th and U concentrations, and long time periods below annealing temperatures (Sanborn et al., 2000; Geisler et al., 2003; Rayner et al., 2005; Geisler et al., 2007). Non-formula elements, such as Ca, Al, Mg, and Fe can be enriched and Pb is often lost in the zircons due to alteration. REE compositions in the zircons can be also modified causing light REE (LREE) enrichment (Hoskin, 2005; Cavosie et al., 2006).

The oxygen isotope ratio of zircon ($\delta^{18}O$) is a powerful tool to characterize parental magma, complementing trace element data. Numerous studies show that undamaged zircons can preserve their $\delta^{18}O$ values from the time of crystallization, even through high-grade metamorphism and anatexis (Valley, 2003; Page et al., 2007b; Bowman et al., 2011). Thus, values of $\delta^{18}O$(Zrc) are studied to understand igneous petrogenesis for rocks of all ages (Cavosie et al., 2005; Valley et al., 2005). However, experiments for diffusion rate in zircon indicate that oxygen diffuses faster under hydrous conditions than other common trace elements such as Ti, Th, U and REEs (Cherniak, 2010). While such relatively rapid oxygen exchange has not been documented in natural undamaged zircons, oxygen exchange rate in zircon is likely to be enhanced by radiation damage and thus it is important to estimate the effects of alteration on magmatic $\delta^{18}O$ values.

* Corresponding author. Tel.: +1 608 890 0929; fax: +1 608 262 0693.
E-mail address: saburo@geology.wisc.edu (K. Kitajima).

0009-2541/$ – see front matter © 2012 Elsevier B.V. All rights reserved.
http://dx.doi.org/10.1016/j.chemgeo.2012.09.019

In this paper, we examine the spatially-correlated co-variations of REEs and $\delta^{18}O$ in zircons from rhyolite of the Panorama Formation in the North Pole Dome (NPD), Pilbara Craton, Western Australia with other trace elements such as Ca that are an index of alteration. The goal of this study is to determine if correlations exist for trace elements and $\delta^{18}O$ in zircon at the scale of a 10–25 μm diameter ion microprobe pit, and to test robustness of $\delta^{18}O$ in these zircons, which might have been damaged by radiation.

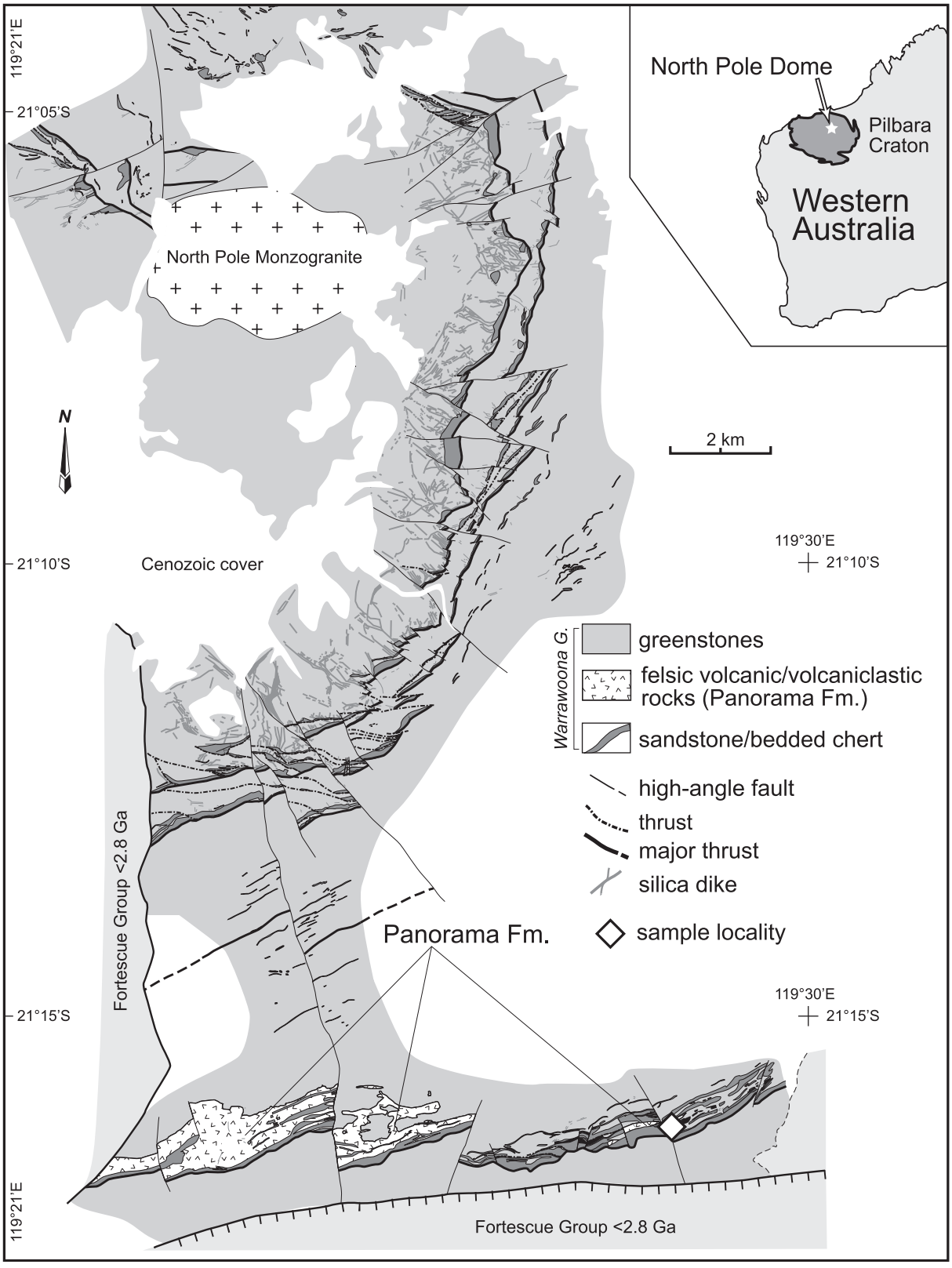

Fig. 1. Geological map of the North Pole Dome in the Pilbara Craton, Western Australia (modified after Kitajima et al., 2008). Sample locality (96NS-410) is shown by an open diamond.

Table 1
Oxygen isotope, Hf and trace element data of the NPD rhyolite zircon at WiscSIMS.

Grain number	#56		#58	#59	#60	#61	#62	#65	#66		#67	#68
core/rim[a]	core	rim	core	core	core	core	core	core	core	rim	core	core
Li	16.1	16.4		3.4	14.9	5.6	4.9	16.3	1.4	18.0	17.6	4.9
P	2547	1316		417	1795	347	238	338	616	784	1077	440
Ca	838.4	446.4		137.0	953.8	21.3	48.1	35.9	85.4	265.7	402.9	83.4
Ti	33.6	19.9		4.3	22.8	3.8	2.9	2.6	3.1	8.7	23.4	4.4
V	8.6	5.0		0.8	13.1	0.2	0.4	0.2	0.3	2.4	3.6	0.6
Fe	681.5	368.7		54.8	875.4	22.4	30.1	57.9	105.7	252.2	416.3	107.8
Y	2490	1655		584	2379	787	830	801	806	1453	1718	893
La	0.32	0.06		0.16	0.07	0.06	0.02	0.02	0.23	0.08	0.03	0.05
Ce	17.7	16.1		10.3	18.4	23.3	12.7	11.9	14.9	18.4	17.5	11.0
Pr	1.2	0.2		0.1	0.3	0.3	0.1	0.1	0.9	0.4	0.1	0.2
Nd	11.1	2.5		1.6	3.4	3.7	2.1	1.0	8.3	5.8	2.2	1.8
Sm	13.0	4.8		1.9	6.4	5.2	3.5	2.4	7.8	7.9	4.5	4.2
Eu	12.8	6.5		1.6	8.5	2.8	1.2	0.8	4.1	4.5	6.2	2.4
Gd	78	50		13	61	20	19	14	22	43	48	20
Tb	50	33		7	45	7	9	6	9	21	32	11
Dy	403	256		60	359	72	84	62	84	166	247	100
Ho	98	62		20	87	26	30	24	28	48	62	31
Er	281	183		79	263	106	119	109	108	170	187	117
Tm	50	32		18	50	24	27	25	23	34	37	25
Yb	400	275		169	431	236	253	250	213	307	315	234
Lu	76	52		37	83	49	52	54	45	63	61	47
Hf	13530	13333		12900	13400	11600	13200	14200	13100	13500	12900	13600
Th	235	192		76	207	124	126	119	114	229	182	101
U	393	319		163	393	187	227	300	209	316	351	244
ΣREE	1492	972		418	1416	576	612	561	568	890	1020	605
Th/U	0.60	0.60		0.47	0.53	0.66	0.56	0.40	0.54	0.73	0.52	0.41
$(Sm/La)_N$	66	127		19	147	146	310	154	54	148	240	145
$(La/Yb)_N$ [$\times 10^{-4}$]	5.48	1.52		6.45	1.12	1.68	0.50	0.69	7.57	1.91	0.65	1.36
Ce/Ce^*	6.98	40.50		16.02	30.88	40.99	73.57	60.34	7.81	23.14	65.07	26.97
Eu/Eu^*	1.22	1.29		0.97	1.31	0.83	0.46	0.39	0.95	0.74	1.29	0.78
Dy/Dy^*	2.16	2.13		1.45	2.24	1.18	1.36	1.20	1.31	1.47	2.01	1.59
REE type[b]	2	1		1	1	1	1	1	2	1	1	1
Ti-in-zircon thermometer [°C][c]	860	805		671	819	662	642	634	647	729	822	674
$\delta^{18}O \pm 2SD$ [‰ VSMOW]	5.73 ± 0.37	5.84 ± 0.30[d]	5.60 ± 0.37	5.80 ± 0.37	5.65 ± 0.37	5.89 ± 0.37	5.88 ± 0.37	5.51 ± 0.37	5.61 ± 0.37	6.04 ± 0.30[d]	5.74 ± 0.37	5.93 ± 0.37
$^{207}Pb/^{206}Pb$ Age [Ma ± 2σ][e]	3609 ± 39			3425 ± 39	3377 ± 40	3489 ± 40	3295 ± 40				3350 ± 57	3702 ± 55
Concordance [%][e]	101.6			94.5	92.2	94.5	83.1				95.0	98.0
Radiation dose [$\times 10^{15}$ event/mg]	8.35			3.11	7.37	3.78	4.11				6.51	5.30
Stage of radiation damage[f]	III			II	II	II	II				II	II

2. Geological background

The lower part of the Warrawoona Group (3.46 Ga) of the Pilbara Supergroup is extensively exposed in the NPD, Pilbara Craton (Fig. 1) (Van Kranendonk et al., 2001), and consists of an approximately 6 km-thick pile of pillowed basaltic greenstones. The structurally lower part of the NPD is mainly composed of greenstones, thick cherts and interbedded barites. In the upper part, komatiitic greenstones are dominant and minor felsic volcanic rocks of the Panorama Formation occur. Felsic volcanic rocks of the Panorama Formation in the NPD are mainly composed of volcaniclastic and volcanic rocks, and minor tuff, volcanic sandstone and bedded cherts. Felsic volcanic rocks show dacitic to rhyolitic composition (Cullers et al., 1993; Smithies et al., 2007) with quartz and feldspar phenocrysts. In the southeastern part of the NPD, felsic volcanic rocks gradually shift to tuff-tuffaceous sandstones, and some volcaniclastic sandstones preserve cross-lamination.

Two distinct U–Pb age groups (~3.3–3.5 Ga and 3.6–3.7 Ga) are reported for zircons from the NPD rhyolites and the eruption age is disputed (Thorpe et al., 1992; Van Kranendonk, 2006; Kitajima et al., 2008). Kitajima et al. (2008) also reported REE compositions of zircons from the NPD rhyolite. Chondrite-normalized REE patterns of NPD rhyolite zircons are enriched in middle–heavy REE (M–HREE) with relatively flat HREE.

3. Sample and preparation

In this study, we analyzed the same zircon grains used in the LA-ICP-MS geochronology and trace element study of Kitajima et al. (2008). These zircons were separated from 120 g of rhyolite and mounted in a 8 mm diameter epoxy disk for U–Pb and REE analysis using LA-ICP-MS by Kitajima et al. (2008). The sample is a rhyolite (96NS-410) from the Panorama Formation in the southern flank of the NPD (Fig. 1), which was collected from the same horizon as the sample reported by Thorpe et al. (1992). The dated zircons show two U–Pb age groups (~3.3–3.5 Ga and 3.6–3.7 Ga) (Kitajima et al., 2008).

#68	#69	#71		#72		#73		#74		#75	#76	
rim	Core	core	rim	core	rim	core	rim	core	rim	core	core	rim
10.5	9.2	12.2	8.7		11.7			18.0	1.9	9.3	15.8	
718	209	760	618		766			775	234	561	1188	
217.1	12.5	203.8	276.6		328.8			157.7	35.7	127.2	492.1	
8.2	4.0	11.7	5.6		13.1			11.2	1.7	5.6	14.4	
2.1	0.1	1.5	2.4		3.0			1.4	0.1	1.7	4.3	
180.8	33.7	243.8	251.0		448.4			239.1	48.6	108.4	314.0	
1095	690	1211	854		1066			3093	323	1028	1544	
0.22	0.10	0.01	0.10		0.03			0.08	0.11	0.09	0.03	
14.7	16.7	13.9	12.6		14.7			19.5	7.3	16.0	17.1	
0.9	0.1	0.1	0.2		0.1			0.8	0.3	0.2	0.2	
7.5	1.9	2.1	1.9		1.8			13.2	3.5	2.9	2.3	
6.6	2.8	3.9	2.8		3.8			22.4	3.1	4.8	4.9	
5.0	0.9	3.1	2.1		3.9			9.4	1.9	2.7	4.8	
30	14	29	21		30			96	9	26	42	
16	6	16	12		19			36	4	13	25	
136	56	131	98		153			300	31	106	174	
38	22	39	26		39			99	10	33	45	
135	95	133	96		122			385	40	122	149	
29	22	29	20		23			80	9	27	32	
258	199	262	182		192			680	86	245	261	
53	44	55	37		39			135	18	52	55	
12800	12000	12300	14500		13100			9300	14500	12500	11700	
108	121	134	145		244			334	52	144	164	
238	218	299	259		320			350	147	256	278	
729	480	716	512		642			1876	221	650	813	
0.45	0.56	0.45	0.56		0.76			0.96	0.35	0.56	0.59	
47	47	417	45		202			450	46	84	254	
6.02	3.31	0.40	3.81		1.09			0.81	8.59	2.61	0.81	
7.70	34.52	83.70	20.65		62.16			18.99	9.35	25.53	57.00	
1.08	0.43	0.88	0.83		1.12			0.61	1.10	0.73	1.01	
1.62	1.18	1.59	1.67		2.00			1.17	1.18	1.43	1.62	
1	1	1	1		1			1	1	1	1	
724	666				765			751	606	693	774	876
	5.96 ± 0.062	5.59 ± 0.62		5.53 ± 0.62	5.99 ± 0.30[d]	5.79 ± 0.62	5.61 ± 0.62	6.33 ± 0.30[d]	5.93 ± 0.30[d]	5.43 ± 0.62	5.60 ± 0.30[d]	5.50 ± 0.30[d]
	3422 ± 56	3636 ± 55				3410 ± 56		3378 ± 56		3275 ± 57	3335 ± 52	
	91.0	97.0				98.9		83.5		73.1	87.7	
	4.20	6.30						7.00		4.60	5.16	
	II	II						II		II	II	

(continued on next page)

For this study, the original epoxy disk was re-cast in the center of a 25 mm epoxy mount with KIM-5 standard zircon (Valley, 2003). Laser ablation craters on the zircon surface for U–Pb and REE analysis were nearly removed by regrinding and polishing. Because of the depth of the laser pits, this entailed deep grinding and many of the zircons dated by Kitajima et al. (2008) were lost. Topography at the sample surface was checked by profilometer in advance of SIMS analysis and was less than 1 μm. The sample mount was coated with carbon for SEM/CL imaging and SIMS analysis.

4. Methods

4.1. Oxygen isotope analysis

Oxygen-isotope ratios ($^{18}O/^{16}O$) of the rhyolite zircons were measured by CAMECA IMS-1280 ion microprobe in the WiscSIMS Laboratory at the University of Wisconsin-Madison. Analytical procedures are similar to Kita et al. (2009). Oxygen isotopes were analyzed using a 2.0–2.2 nA primary Cs^+ beam with ~10 μm spot size. Secondary ^{16}O and ^{18}O ions were measured simultaneously using two Faraday cup detectors. Oxygen isotope data were acquired during two separate analytical sessions (before and after a trace element analysis session). Chips of KIM-5 zircon ($\delta^{18}O = 5.09$ ‰ VSMOW, Valley, 2003) were used as a standard, and the average value of eight standard analyses bracketing each 10–15 analyses of unknowns was used to correct for instrumental bias. The precision of individual analyses is estimated by two standard deviations (2SD) of the reproducibility of bracketing standard analyses and averages 0.3 ‰ (Valley and Kita, 2009).

4.2. Hafnium and trace elements

Rare earth elements (REE: La–Lu) and ten other trace elements (Li, P, Ca, Ti, V, Fe, Y, Hf, Th and U) were measured using a CAMECA IMS-1280 in the WiscSIMS laboratory at the UW-Madison between

Table 1 (*continued*)

Grain number	#77		#78		#79		#80	#81	#82	#83		#84		#85
core/rim[a]	core	rim	core	rim	core	rim	core	core	core	core	rim	core	rim	core
Li	16.4	8.5	25.2	16.2	14.6	11.4	10.0	8.9	10.7	23.1	18.4	19.2	10.2	0.4
P	1897	814	1829	673	4076	1504	1111	244	1060	3529	683	1470	813	203
Ca	738.2	184.4	777.4	287.4	1613.6	524.8	313.6	79.3	405.0	1391.5	263.5	629.3	170.1	3.7
Ti	38.9	21.3	34.1	10.9	59.1	20.6	11.1	3.1	18.5	96.7	9.1	28.8	11.1	2.7
V	7.7	2.7	6.2	2.5	15.2	6.1	2.9	0.7	5.6	10.5	2.2	6.0	1.9	0.1
Fe	518.6	233.1	655.4	235.5	1213.2	448.4	273.6	47.5	295.0	2557.2	306.9	440.1	176.0	5.0
Y	3098	1419	2461	1177	4261	1655	1245	955	1269	4420	1038	2070	1004	579
La	0.07	0.05	0.08	0.04	0.11	0.04	0.15	0.19	0.10	0.19	0.02	0.08	0.06	0.01
Ce	14.7	14.2	19.6	13.9	21.1	13.3	14.3	16.6	13.4	35.2	16.8	14.8	16.7	9.4
Pr	0.3	0.2	0.3	0.1	0.5	0.3	0.6	0.2	0.3	0.5	0.1	0.2	0.2	0.1
Nd	4.8	3.5	3.2	1.3	5.4	3.4	5.7	3.7	3.5	7.4	1.8	2.9	2.0	1.1
Sm	12.0	6.0	6.8	3.2	12.4	5.0	7.4	5.2	5.1	16.3	3.4	6.9	3.3	2.4
Eu	17.2	5.8	7.8	3.1	15.2	5.1	5.2	1.8	5.3	24.6	2.8	6.7	2.4	0.5
Gd	119	50	69	30	128	52	37	25	40	133	25	61	25	12
Tb	66	24	44	17	84	28	21	11	24	93	16	39	15	4
Dy	459	180	342	139	605	190	168	100	181	772	136	296	126	48
Ho	106	47	83	38	136	45	43	32	42	176	37	71	36	17
Er	311	160	250	126	391	137	146	129	136	482	126	215	125	79
Tm	54	33	48	28	71	28	27	27	24	82	24	38	25	17
Yb	432	279	386	234	536	225	246	251	221	641	217	343	225	173
Lu	83	58	73	48	98	44	48	51	42	107	44	66	48	38
Hf	11900	13700	11600	12400	9900	12200	13100	13400	13200	12800	13500	13500	12700	13000
Th	228	185	221	121	276	177	131	154	136	909	212	180	132	69
U	404	321	445	299	493	339	221	229	230	1024	332	308	262	156
ΣREE	1678	860	1333	681	2104	777	771	653	738	2571	651	1161	650	401
Th/U	0.57	0.58	0.50	0.40	0.56	0.52	0.59	0.67	0.59	0.89	0.64	0.58	0.50	0.44
$(Sm/La)_N$	278	204	127	132	176	187	80	44	81	140	334	144	85	398
$(La/Yb)_N$ [$\times 10^{-4}$]	1.10	1.17	1.52	1.16	1.46	1.32	4.14	5.23	3.13	2.01	0.53	1.54	1.90	0.38
Ce/Ce*	23.94	33.64	29.61	50.31	22.02	29.47	11.47	22.36	17.95	27.17	112.86	26.08	36.90	98.42
Eu/Eu*	1.38	1.02	1.09	0.96	1.15	0.95	0.96	0.47	1.13	1.61	0.92	0.98	0.79	0.32
Dy/Dy*	1.85	1.50	2.00	1.68	2.09	1.64	1.79	1.36	1.93	2.46	1.93	2.04	1.76	1.24
REE type[b]	1	1	1	1	1	1	1	1	1	1	1	1	1	1
Ti-in-zircon thermometer [°C][c]	812		862	748	925	809	750	647	798	989	733			638
δ18O ± 2SD [‰ VSMOW]	5.50 ± 0.30		5.68 ± 0.62[d]	5.27 ± 0.62	5.98 ± 0.30[d]	6.01 ± 0.30[d]		5.86 ± 0.30[d]	6.08 ± 0.30[d]	5.87 ± 0.30[d]				
$^{207}Pb/^{206}Pb$ Age [Ma ± 2σ][e]	3349 ± 52						3660 ± 50	3355 ± 52	3271 ± 52	3374 ± 52		3678 ± 50		
Concordance [%][e]	94.0						99.9	97.1	59.6	93.9		90.0		
Radiation dose [×1015 event/mg]	7.52						4.83	4.35	4.13	20.3		6.8		
Stage of radiation damage[f]	II						II	II	II	III		II		

Note: Concentrations in ppm. Th/U values are calculated by using measured (not corrected by age) values. $Ce/Ce^* = Ce_N/(La_N \times Pr_N)^{1/2}$, $Eu/Eu^* = Eu_N/(Sm_N \times Gd_N)^{1/2}$, $Dy/Dy^* = Dy_N/(Tm_N^2 \times Gd_N^3)^{1/5}$. Oxygen isotope analysis sessions were carried out on March 2010 (1) and July 2010 (2).

[a] Core and rim represent inner and outer portion of zircons, respectively.

[b] REE type is defined by Cavosie et al. (2006).

[c] Temperatures were estimated using an equation by Watson and Harrison (2005) with no activity correction.

[d] Weighted average of multiple analyses and 2SD.

[e] Data from Kitajima et al. (2008).

[f] Stage of radiation damage from Murakami et al. (1991).

the two oxygen-isotope sessions. Analytical procedures are similar to Page et al. (2007a) and Bouvier et al. (2012). Hafnium and trace elements were measured in single collector mode by axial electron multiplier using magnetic peak switching. In order to minimize molecular interference between REE and REE-oxide peaks, a 40 V energy offset was applied to the sample and mass-resolving power (M/ΔM at 10 % height) was set to 3000. All analyses consisted of 100 s pre-sputtering followed by seven mass scans. After these analyses, we checked all ion microprobe pits by SEM and rejected some spots due to the pit condition (e.g., analysis pit on a crack, epoxy, or a mineral inclusion).

5. Results

Results of oxygen isotope, Hf and trace element analyses for rhyolite zircons from NPD are summarized in Table 1 with U–Pb geochronology data reported by Kitajima et al. (2008). Full tables of sample and standard analyses of oxygen isotopes are reported in Supplementary Table S1. SEM/CL images of zircons from the NPD rhyolite exhibit oscillatory, igneous zoning, no inherited cores, and no metamorphic overgrowths (Fig. 2). We analyzed cores (inner portion of zircon) and rims (outer portion) in the zircons by SIMS. The pits in cores are directly beneath the former LA-ICP-MS spots for U–Pb dating and in the center of the igneous zoning recognized by CL. The rims are located outside of the "core" spot and in general do not overlap the LA-ICP-MS spots.

5.1. Oxygen isotope ratios

We carried out *in-situ* $\delta^{18}O$ measurement on 48 spots from 23 grains during two sessions; nine grains have at least one spot/each, core and rim (Fig. 3). The range of $\delta^{18}O$ for single spots on NPD rhyolite zircons is 5.3–6.4 ‰, and the average is 5.78 ± 0.46 ‰ (2SD, n = 48; 2SE = 0.07 ‰). Averages of $\delta^{18}O$ on cores and rims are indistinguishable at 5.75 ± 0.42 ‰ (n = 23) and 5.76 ± 0.50 ‰ (n = 9), respectively. There is no systematic difference in $\delta^{18}O$ values between core and rim of single grains (see Supplementary Fig. S1), so we

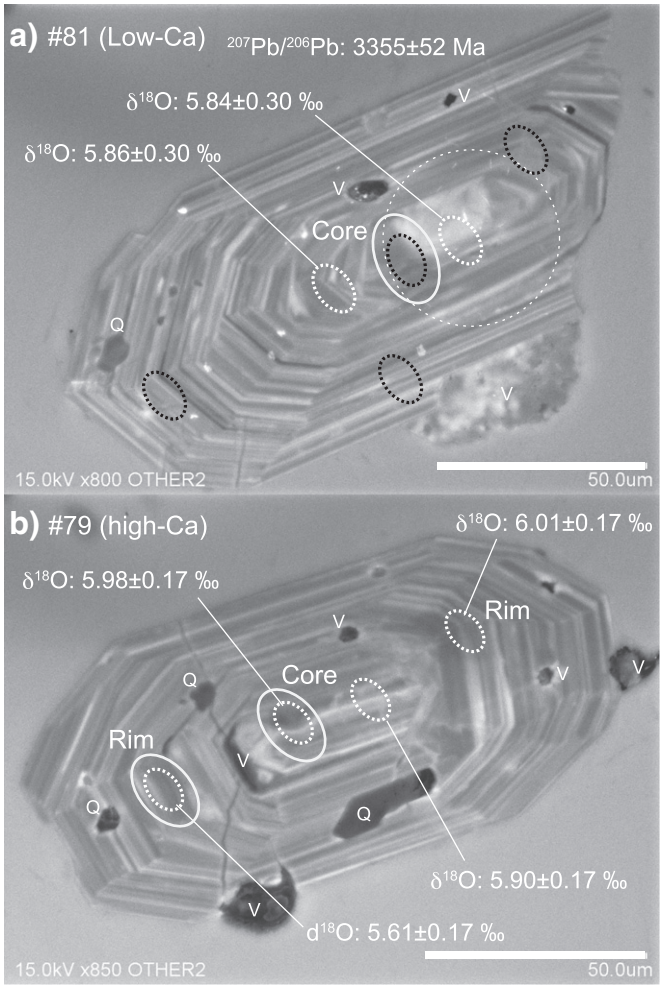

Fig. 2. Cathodoluminescence (CL) images of NPD rhyolite zircons which are typical examples of (a) low-Ca (<120 ppm; #81) and (b) high-Ca (≥120 ppm; #79) grains. Solid and dashed ovals are the locations of analysis pits for trace elements and oxygen isotope ratio, respectively, measured at WiscSIMS. Black dashed ovals are rejected spots (see Table S1 for details). White dotted circles represent analysis spots of U–Pb analysis by LA-ICP-MS (Kitajima et al., 2008). Light gray inclusions are quartz (Q), and black ones are voids (V). Scale bars are 50 μm.

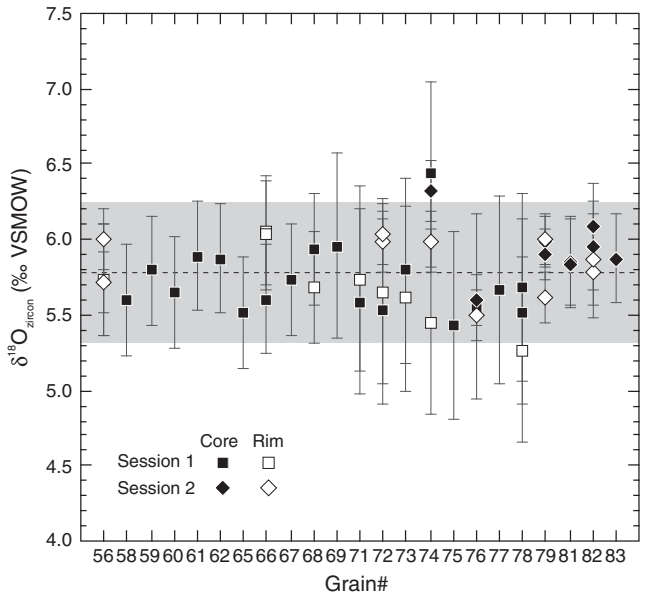

Fig. 3. Values of $\delta^{18}O$ in 23 zircon grains from NPD rhyolite. The data are combined from two separate sessions at WiscSIMS: Session 1 (squares) and Session 2 (diamonds). Spots at the core of a zircon are shown as solid and rims are open symbols. There is no systematic difference in $\delta^{18}O$ between Session 1 and Session 2. The dashed line indicates the average $\delta^{18}O$ value (5.78 ± 0.46 ‰ [2SD]) of all plotted data (n = 48). The error bars are 2SD.

will discuss $\delta^{18}O$ values on core/rim with no distiction. Averages of $\delta^{18}O$ values on younger (3.3–3.5 Ga) and older (3.6–3.7 Ga) grains are also indistiguishable at 5.82 ± 0.44 ‰ and 5.75 ± 0.34 ‰, respectively (see Supplementary Fig. S2), and we will also discuss the $\delta^{18}O$ values of younger/older grains with no distinction.

5.2. Hafnium and trace elements

Hafnium and 23 trace elements were analyzed (Li, P, Ca, Ti, V, Fe, Y, Th, U, and REEs) by ion microprobe at WiscSIMS, and concentrations of each element in the NPD rhyolite zircon are summarized in Table 1. Average, minimum and maximum values for cores and rims are summarized in Table 2, and analyses are classified as Type-1 and Type-2 based on chondrite-normalized LREEs: Type-1 (La_N<1 and Pr_N<10) and Type-2 (La_N>1 and Pr_N>10) (Cavosie et al., 2006). For single grains, some cores are enriched relative to rims in trace elements other than Hf, Th and U (Supplementary Fig. S3). There is, however, no systematic difference between all core and rim data. Hereafter, we will discuss data without distinction of cores and rims, except that we use only core values when comparing to previous geochronology data (Kitajima et al., 2008), because those data are from cores. There is no systematic difference in Hf and trace element compositions on younger/older grains, thus we will discuss them with no distinction as well as oxygen isotopes.

Rayner et al. (2005) reported that unaltered zircons from a 2.9 Ga granitic dike from the Acasta Gneiss Complex, Slave Province have less than 120 ppm by weight ("ppm by weight" will hereafter be shortened to "ppm") of Ca. We also classified the analysis spots depending on Ca concentration in zircon into low-Ca spots ([Ca]<120 ppm) and high-Ca spots ([Ca]≥120 ppm). The majority (74%) of NPD rhyolite zircons are high-Ca spots, above the level suggested for unaltered zircon.

Chondrite-normalized REE patterns of the NPD rhyolite zircons are shown in Fig. 4. Type-2 patterns data show a number of features including flatter slopes of LREE and smaller Ce anomalies (Ce/Ce*) (Hoskin, 2005; Cavosie et al., 2006). Two zircons (#56, #66) have distinct Type-1 and Type-2 domains within the single grain (Table 1). Most high-Ca zircons show unusual enrichment between Tb and Ho, with concave downward M–HREE chondrite-normalized patterns (Fig. 4b), and low-Ca zircons represent low total REE concentrations with smooth M-HREE patterns (Fig. 4a).

We plotted REE data of the NPD rhyolite zircons on a $(Sm/La)_N$ vs. [La] diagram (Hoskin, 2005) to distinguish hydrothermal from magmatic zircon (Fig. 5a). All NPD rhyolite zircons plot in the magmatic field. Fig. 5b–d are empirical discrimination diagrams that distinguish zircons with parent rocks from continental vs. oceanic crust (Grimes et al., 2007). The NPD rhyolite zircons plot in the field of continental crust for all diagrams: [U] vs. [Yb] (Fig. 5b), U/Yb vs. [Hf] (Fig. 5c) and U/Yb vs. [Y] (Fig. 5d). We also plotted ranges of Archean TTG zircons (Bouvier et al., 2012). Both types of zircon from the NPD rhyolite and Archean TTG overlap, but the NPD rhyolite zircons plot slightly higher in Y and HREE (Fig. 5a, b, d).

There is a strong positive correlation between Ca and P in the NPD rhyolite zircons (Fig. 6). The regression line of P vs. Ca plot has a slope of approximately P/Ca = 3/1 (atomic ratio). All other analyzed trace elements in the NPD rhyolite zircon except Hf also correlate with Ca to various degrees and selected elements are shown in Fig. 7a–g. Concentrations of Ti, Fe, total REE (ΣREE), Th and U show clear positive correlations with [Ca]. Hafnium and concordance of U–Pb ages have

Table 2
Summary of Hf and trace elements data of the NPD rhyolite zircon.

	Type-1						Type-2		
	Core (n=21)			Rim (n=11)			Core (n=2)		
	Min	Max	Average	Min	Max	Average	Min	Max	Average
Li	0.4	25.2	12.4	1.9	18.4	12.0	1.4	16.1	8.8
P	203	4076	1122	234	1504	811	616	2547	1581
Ca	3.7	1613.6	410.8	35.7	524.8	272.8	85.4	838.4	461.9
Ti	2.6	96.7	19.2	1.7	21.3	11.8	3.1	33.6	18.3
V	0.1	15.2	3.9	0.1	6.1	2.8	0.3	8.6	4.4
Fe	5.0	2557.2	405.2	48.6	448.4	268.1	105.7	681.5	393.6
Y	579	4420	1710	323	1655	1158	806	2490	1648
Hf	9300	14200	12476	12200	14500	13294	13100	13530	13315
Th	69	909	197	52	244	163	114	235	175
U	156	1024	323	147	339	286	209	393	301
ΣREE	401	2571	1007	221	972	690	568	1492	1030
Th/U	0.40	0.96	0.57	0.35	0.76	0.55	0.54	0.60	0.57
Ce/Ce*	11.47	98.42	38.70	7.70	112.86	38.79	6.98	7.81	7.39
Eu/Eu*	0.32	1.61	0.89	0.74	1.29	0.98	0.95	1.22	1.09
Dy/Dy*	1.17	2.46	1.66	1.18	2.13	1.69	1.31	2.16	1.74

Note: Concentrations in ppm. Th/U values are calculated by using measured (not corrected by age) values. $Ce/Ce^* = Ce_N/(La_N * Pr_N)^{1/2}$, $Eu/Eu^* = Eu_N/(Sm_N * Gd_N)^{1/2}$, $Dy/Dy^* = Dy_N/(Tm_N^2 * Gd_N^3)^{1/5}$.

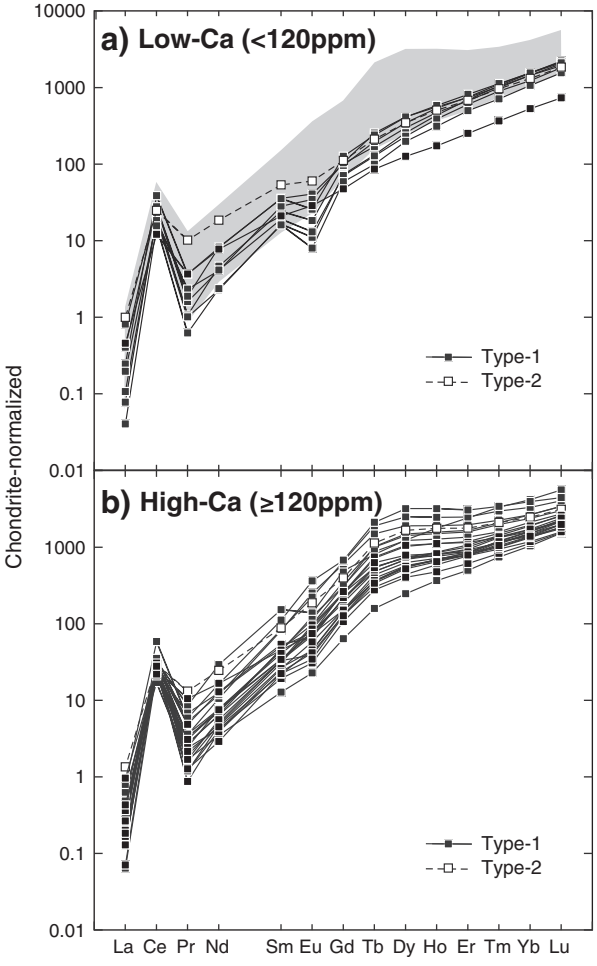

Fig. 4. Chondrite-normalized REE patterns of the NPD rhyolite zircons. Upper diagram shows REE patterns of low-Ca (<120 ppm) zircons (a) and lower diagram shows those of high-Ca (≥ 120 ppm) zircons (b). Low-Ca spots, less than 120 ppm which is the maximum value of unaltered zircons reported in 2.9 Ga zircons by Rayner et al. (2005), have low REE concentration and recognizable Eu-anomalies. REE patterns of high-Ca spots have wide variation of enrichment in M–HREE (Tb, Dy and Ho) concentration. Type-2 zircon domains are defined by enrichment in LREE (Cavosie et al., 2006). Shaded area in low-Ca plot (a) represents range of high-Ca zircons.

no correlation with Ca (Fig. 7e, i). A negative correlation between Hf and Ti in zircon has been reported previously (Fu et al., 2008; Claiborne et al., 2010), but is not observed in the NPD rhyolite zircons (Fig. 7k).

6. Discussion

6.1. Middle–heavy REE enriched (concave-down) REE patterns

Chondrite-normalized REE patterns of the NPD rhyolite zircons are consistent with those previously analyzed by LA-ICP-MS (Kitajima et al., 2008). Low-Ca spots (<120 ppm) show low ΣREE (Fig. 7d), relatively large Eu anomalies (Eu/Eu*), and linear trends for middle–heavy REEs (M–HREEs) (Fig. 4). On the other hand, high-Ca spots are mostly higher in REE concentration and are relatively enriched from Tb to Er, forming a concave-down hump in the M–HREEs.

Apatite which shows M–HREE concave-down REE pattern has been reported from veins which are composed of very fine-grained silica in the NPD (Nishizawa et al., 2004). These authors conclude that the apatites were precipitated from fluid with M–HREE enriched compositions. This result suggests the possibility that the NPD rhyolite has been also subjected alteration by aqueous fluid enriched in P, Ca and M–HREE.

In order to make a quantitative estimation of the M–HREE hump in the NPD rhyolite zircon, we estimated the Dy anomaly (Dy/Dy*). Dy* was calculated by following equation:

$$Dy^* = \left[(Tm_N)^2 \times (Gd_N)^3\right]^{1/5} \quad (1)$$

where Tm_N and Gd_N are chondrite-normalized values in zircon. This equation assumes that the normal chondrite-normalized REE pattern from Gd to Tm is linear and values increase in logarithmic scale. Calculated Dy/Dy* anomalies range from 1.17 to 2.46, and show a good positive correlation with [Ca] (Fig. 8). This correlation suggests that the enrichment of REE, especially M–HREEs, and Ca occurred due to alteration of domains within individual zircons. Thus, the NPD rhyolite zircons are modified not only in ΣREE, but also in the shape of REE pattern by alteration. Likewise, LREE can be added to altered zircons and LREE enrichment in the zircon as reported (Hoskin, 2005; Cavosie et al., 2006). The enrichment in M–HREEs which is dominant in the NPD rhyolite zircon, is uncommon in the Precambrian and Phanerozoic zircons (Hoskin and Schaltegger, 2003), and might

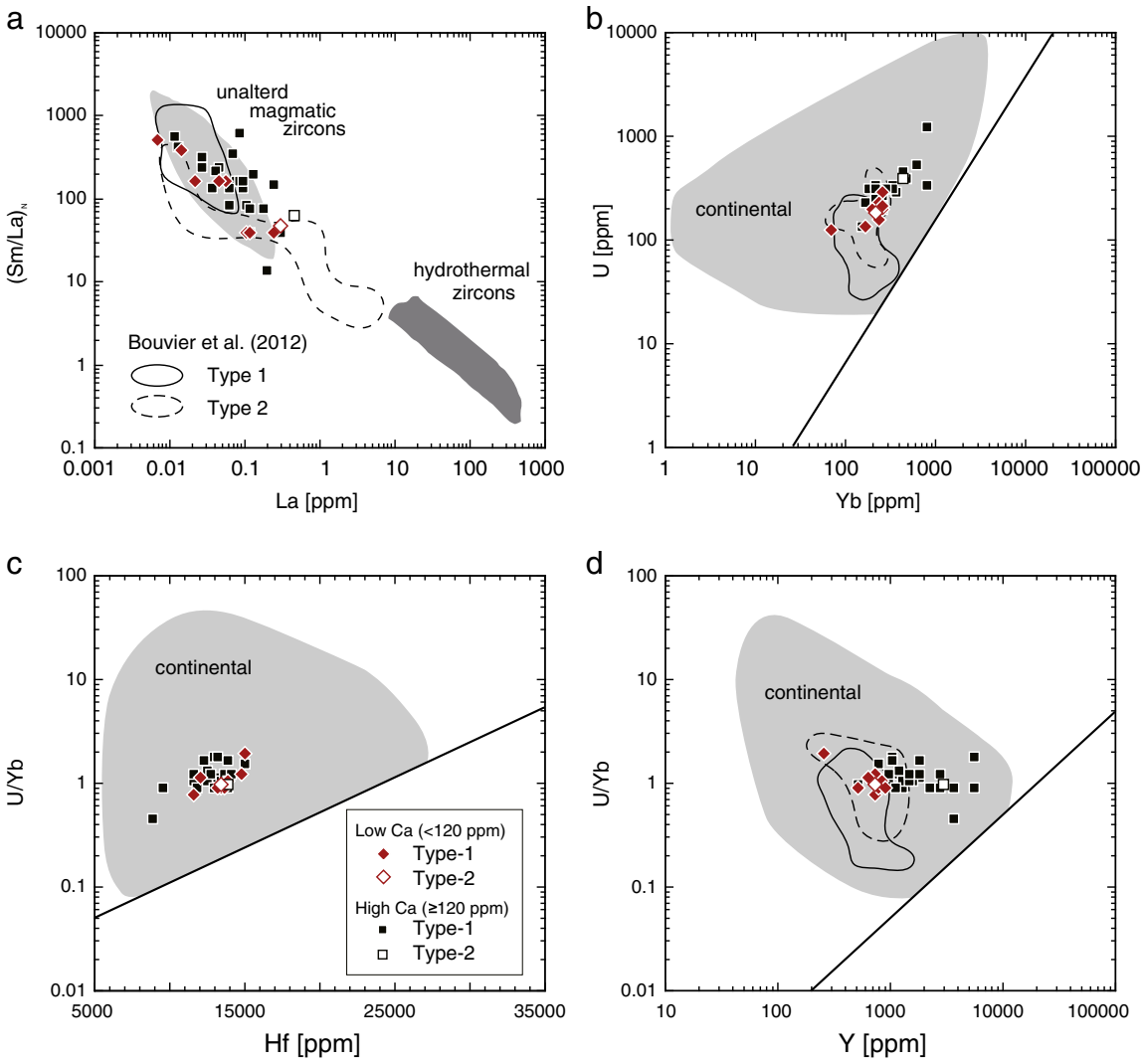

Fig. 5. Geochemical discriminant diagrams for the NPD rhyolite zircons. $(Sm/La)_N$ vs. La (ppm) of the NPD zircons (a). Shaded fields are unaltered magmatic and hydrothermal zircons from Hoskin (2005). NPD zircons plot in the continental-crust fields in U (ppm) vs. Yb (ppm) (b), U/Yb vs. Hf (ppm) (c) and U/Yb vs. Y (ppm) (d) are from Grimes et al. (2007). Heavy lines indicate the lower limit of zircons from continental crust. The compositional variations of Archean TTG zircon (Bouvier et al., 2012) are plotted by solid (Type-1) and dashed (Type-2) lines (a, b and d).

indicate differing fluid compositions from the relatively common LREE enrichment alterations.

6.2. Phosphorus- and calcium-rich mineral inclusions?

The positive correlation between Ca and P in the NPD rhyolite zircons has a slope of ~3 in atomic ratio with $R^2 = 0.959$ (Fig. 6). After Hf and trace element analysis, we checked the ion microprobe pits using SEM/BSE and no μm-scale mineral inclusions are observed in the pits. Quartz is the most common mineral inclusion in these zircons, but was observed by SEM before analysis and avoided during SIMS analysis (Fig. 2). A few uncommon inclusions of apatite up to 1–15 μm in diameter were observed in polished zircon surfaces, though only outside of the SIMS pits in NPD rhyolite zircons.

If inclusions are the cause of the P/Ca correlation in Fig. 6, then the contaminant is indicated to have a stoichiometry of P/Ca = ~3/1. However, apatite is the only phosphate found in NPD zircons and has been reported as a secondary mineral caused by hydrothermal alteration (Nishizawa et al., 2004). The atomic ratio of P/Ca in apatite, $Ca_5(PO_4)_3(OH)$, is 3/5, which does not explain the NPD data (Fig. 6). Furthermore the trend in Fig. 6 has an intercept (Ca = 0) at ~1.21×10^{-3} atoms per formula unit (a.p.f.u) P or 204 ppm, which shows that at least some P is present in Ca-poor zircons, presumably by "xenotime-type" substitution. Internal precision of Ca for all analyses shows relatively low values (±7.0 %, averaged 2SE of all analyses) in zircon and there is no significant difference between samples and the NIST610 running standard (±4.8 %, averaged 2SE of 4 analyses). In the NPD rhyolite zircon, 2SE for Ca shows no correlation with [Ca] (see Supplementary Fig. S4). Thus, it is concluded that the Ca and P contents measured in zircons are not the result of μm-scale mineral inclusions.

6.3. Ca and other trace element concentrations in the NPD rhyolite zircons

Calcium and certain other trace elements (Al and Fe) are usually at very low concentration (maximum of a few hundred ppm) in unaltered igneous zircons, but they may be higher in altered zircon (Hoskin and Schaltegger, 2003). In the NPD rhyolite zircons, calcium correlates with other trace elements including ΣREE (Fig. 7). These correlations suggest that concentrations of these trace elements in zircon were modified by secondary alteration, and that they may substitute in non-lattice domains due to radiation damage that did not exist at the time of magmatic

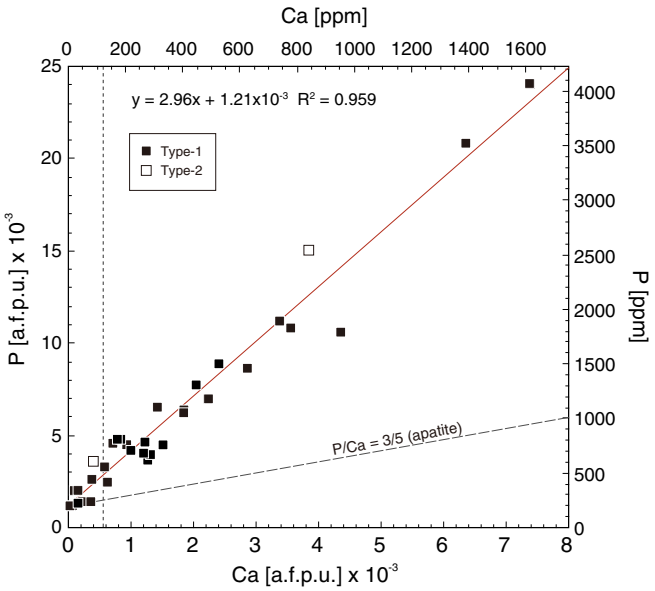

Fig. 6. Phosphorus (atoms per formula unit: a.p.f.u) vs. Ca (a.p.f.u.) in the rhyolite zircons from the NPD. Solid heavy line is a regression using all data with a formula: $y = 2.96x + 1.21 \times 10^{-3}$, $R^2 = 0.959$. This line indicates a relation between P and Ca with 3/1 in atomic ratio. The dashed line is the 3/5 atomic ratio of apatite.

crystallization (Utsunomiya et al., 2007). Some trace elements, however, also can be in ionic substitutions within the zircon crystal lattice, formed during crystallization (Finch et al., 2001; Hoskin and Schaltegger, 2003), and they might preserve igneous compositions in less altered domains.

Lithium concentration in the NPD rhyolite zircons does not show a clear correlation with Ca (Fig. 7a). Lithium can be in ionic substitution in zircon (Finch et al., 2001; Ushikubo et al., 2008; Bouvier et al., 2012). The zircons from continental crust have higher concentration (1–100 ppm) of Li than zircons from oceanic crust or the mantle (Ushikubo et al., 2008; Grimes et al., 2011). The NPD rhyolite zircons range in [Li] from 0.4–25 ppm (Table 2), and this value is comparable to lower values in zircons from continental crust. Lithium and Ca correlate weakly above ~10 ppm Li and ~120 ppm Ca (Fig. 7a). In the low [Li] (<10 ppm) and low Ca (<120 ppm) zircons, the lack of correlation with [Ca] suggests that Li in these zircons was not be affected by the alteration and could preserve original concentration.

Titanium and Ca show a good correlation above [Ca] = 120 ppm in the NPD rhyolite zircons (Fig. 7b) while [Ti] in low-Ca spots is relatively constant (inset in Fig. 7b). This Ti and Ca correlation has not been reported previously. Titanium substitution in zircon correlates with magmatic differentiation and has been calibrated as a geothermometer (Watson et al., 2006) although questions remain (Fu et al., 2008; Hofmann et al., 2009). We calculated temperature for the NPD rhyolite zircon using Ti-in-zircon thermometry with no activity or pressure correction to examine the variation of their crystallization temperature (Table 1). The estimated temperatures vary from 610 to 990 °C. The host rhyolite was quartz-saturated, but no Ti-mineral in known. Thus, low $a(TiO_2)$ could cause temperature estimates to be low while crystallization at less than 1 GPa would cause estimates to be high. This temperature range is relatively large for volcanic rocks and the temperature does not correlate with $^{207}Pb/^{206}Pb$ ages. In high-Ca spots, the positive correlation of [Ti] and temperature with Ca, however, suggests that Ti was added after crystallization by alteration. Titanium positively correlates with U (Fig. 7j). This relation is not consistent with evolution of magma during crystallization (Claiborne et al., 2010) and suggests that at least some trace elements in high-Ca spots in the NPD rhyolite zircons do not reflect magmatic compositions at the time of zircon crystallization.

Unlike [Ti] in the NPD rhyolite zircon, [Hf] does not correlate with [Ca], suggesting no effect of alteration on [Hf], presumably due to the relatively high concentration in zircon and less solubility in aqueous fluid. A negative correlation between Ti and Hf concentration in igneous zircons has been interpreted as the result of magmatic evolution (Claiborne et al., 2010). In contrast, the NPD rhyolite zircons show no correlation between Hf and Ti (Fig. 7k). This lack of correlation further suggests that Ti was added to some NPD rhyolite zircons during subsolidus alteration.

In the NPD rhyolite zircons, U and Th concentrations correlate with Ca (Fig. 7f, g). If U and Th were added during alteration, U–Pb ages must be affected and concordance should correlate with higher [U] and [Ca]. There is, however, no correlation between concordance of U–Pb age and [Ca] (Fig. 7i). This suggests that U concentration in the NPD rhyolite zircons was not affected by alteration and may show igneous concentrations. The correlation with [Ca] can be explained because the U-rich zircons experienced higher α-doses and may have had more radiation damage. The ratios of Th and U (Th/U) in the NPD rhyolite zircons range from 0.4 to 1 (average: 0.57 ± 0.24, 2SD), and the correlation with [Ca] is poor (Fig. 7h). This absence of correlation between [Ca] and Th/U also suggests that Th was not added as the result of alteration. These relations suggest that there is no addition of Th and U by alteration, and that the NPD rhyolite zircons preserve original values of [Th] and [U].

These lines of evidence suggest that in the Ca-rich domains of some zircons, Ca and the other trace elements that have positive correlations (P, Ti in high-Ca spots, Fe and REEs) likely represent secondary alteration rather than original compositions.

6.4. Radiation damage

Chemical alteration in zircons is highly correlated with millimeter- to nanometer-scale domains of radiation damage (Sanborn et al., 2000; Geisler et al., 2003; Utsunomiya et al., 2007). Sanborn et al. (2000) reported that Ca content in zircon from the 2.9 Ga granitic dike in the Acasta gneiss (same sample as Rayner et al., 2005) correlates with the extent of radiation damage measured using Raman spectroscopy and transmission electron microscopy (TEM). Utsunomiya et al. (2007) also reported that alteration in 3.3 Ga zircons from granites exposed near the Jack Hills occurred at micrometer- to nanometer-scale due to radiation damage.

To estimate the degree of radiation damage, the cumulative α-doses in NPD rhyolite zircons were calculated from Th and U concentrations in zircon cores and $^{207}Pb/^{206}Pb$ ages (Kitajima et al., 2008) using the Murakami et al. (1991) equation (Table 1). These doses calibrate radiation damage if there has been little or no annealing. The α-doses range from 3.11 to 20.3×10^{15} events/mg and correlate with [Ca] (Fig. 9a). If not annealed, these doses are equivalent to stage-II ($3–8 \times 10^{15}$ α-decay events/mg, Murakami et al., 1991) except two spots (#56 Core and #83 Core) which belong to stage-III ($>8 \times 10^{15}$ α-decay events/mg). In stage-II, crystalline regions are converted into aperiodic regions due to α-damage but further expansion of the unit cell in the remaining crystalline regions is absent. In stage-III, the zircon is entirely composed of aperiodic regions as can be determined by X-ray or electron diffraction (Murakami et al., 1991). The cumulative α-dose of all NPD rhyolite zircons, if not annealed, is above the first percolation point (2×10^{15} events/mg, Ríos et al., 2000), which would represent continuous connectivity of damaged domains and the possibility of fast pathways for diffusion and element migration within the zircon grain. The correlation between radiation damage and [Ca] suggests that the associated trace element enrichments are accommodated by damaged domains due to the radiation damage. However it is likely that these zircons are at least partly annealed and possible that radiation damage never exceeded the first percolation. The grain with cumulative stage-III radiation dose was elevated in trace elements, but the age of this grain is consistent with other stage-II zircon ages and still preserves the igneous $^{207}Pb/^{206}Pb$

age (Fig. 9b). The absence of correlation among α-dose and $^{207}Pb/^{206}Pb$ ages shows that radiation-enhanced alteration does not necessarily affect the U–Pb system of the NPD rhyolite zircons (Fig. 9b, c). These lines of evidence also support the interpretation that the NPD rhyolite zircons preserve original [Th] and [U] values, which has been discussed above.

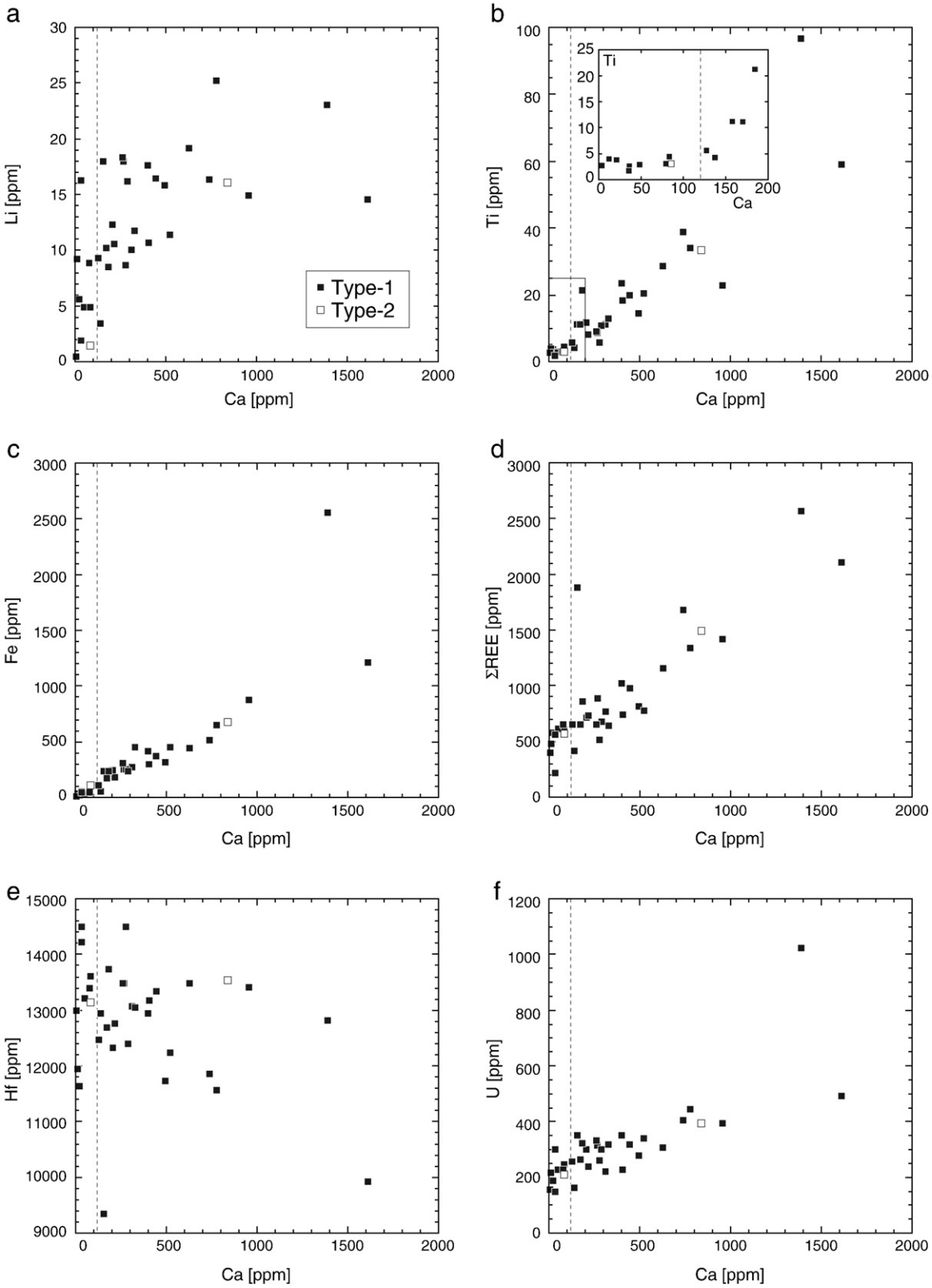

Fig. 7. Calcium (ppm) vs. Li (a), Ti (b), Fe (c), total REE (ΣREE) (d), Hf (e) and U (f), Th (g) in ppm, Th/U (h) and concordance (i) in the NPD rhyolite zircon. Titanium (ppm) vs. U (j) and Hf (k) in ppm. Concordance data are from Kitajima et al. (2008). Dashed lines in a–h represent 120 ppm Ca. Symbols: solid black squares = Type-1 and open squares = Type-2. Titanium, Fe, ΣREE, Th and U correlate with Ca, while Ca vs. Li, Hf and Th/U, and Hf vs. Ti show no correlations.

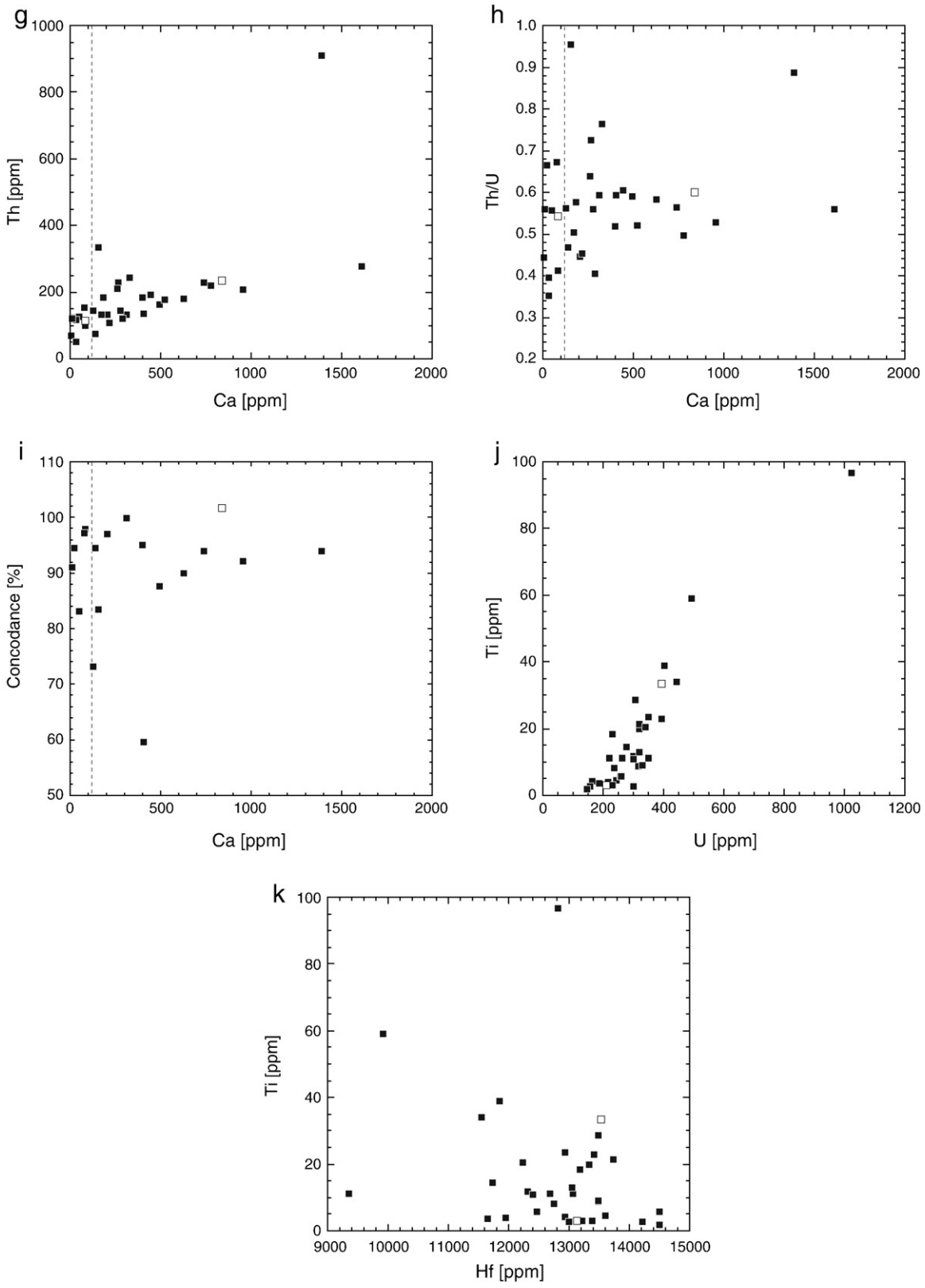

Fig. 7 (*continued*).

The lower intercept of discordia with concordia for the NPD rhyolite zircon is 755 Ma, and zircons from other rock types in the NPD also show similar lower intercept ages (Kitajima et al., 2008). This suggests that a Pb-loss event occurred at ~755 Ma in the NPD. Concordance of U–Pb ages in the NPD zircons, however, does not correlate with [Ca] or cumulative α-dose (Fig. 9c). Thus the alteration involving Ca addition may not relate to the Pb-loss event at ~755 Ma, but may still relate to the cumulative α-dose and more recent alteration.

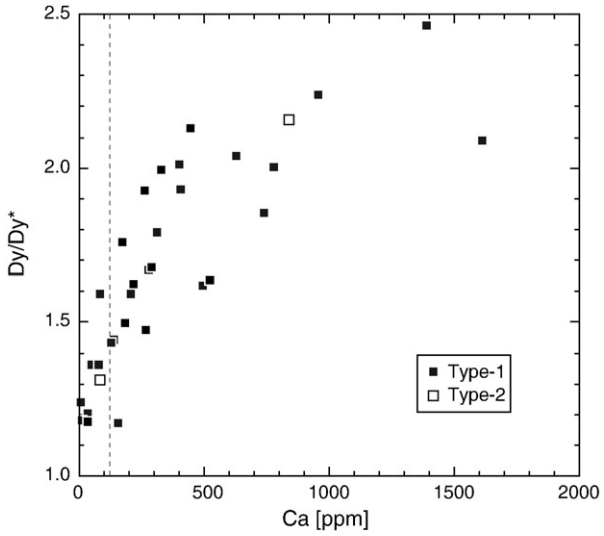

Fig. 8. Dysprosium anomaly (Dy/Dy*) vs. Ca (ppm). Dy anomaly correlates to Ca concentration. See text for the Dy* calculation. Dashed line represents 120 ppm Ca.

6.5. Oxygen isotope ratios in the North Pole Dome rhyolite zircons

Values of $\delta^{18}O$ in the NPD rhyolite zircons are homogeneous at $\delta^{18}O = 5.78 \pm 0.46$ ‰ (2SD, n = 48) (Fig. 3). The variability of these values is the same as analyses on the homogeneous standard, KIM-5 (5.09 ± 0.57 ‰, n = 15 for first session and ± 0.29 ‰, n = 18 for second session) supporting the conclusion that the NPD zircons originally had a tight range in $\delta^{18}O$ and are not altered in $\delta^{18}O$. This value corresponds well with the averages for zircons from 2.74 to 2.67 Ga, unenriched TTG plutons (5.6 ± 1.0 ‰, 2SD, n = 42) and late Archean (~2.7 Ga) felsic volcanics (5.57 ± 0.96 ‰, 2SD, n = 45) in the Superior Province, the Pilbara Craton and elsewhere (Valley et al., 2005). As in many other Archean igneous rocks, the NPD zircons are similar or very slightly higher in $\delta^{18}O$ to the value for igneous zircon in high temperature equilibrium with mantle magma (5.3 ± 0.6 ‰, 2SD) (Valley et al., 1998). If the tight range of $\delta^{18}O$ in NPD rhyolite zircons is the result of exchange by diffusion in undamaged zircon, then very high-grade metamorphism (>800 °C: Page et al., 2007b; Bowman et al., 2011) and high water activity would be necessary. The NPD rhyolite, however, has been subject at most to greenschist facies metamorphism (Terabayashi et al., 2003) and zircons still have igneous, oscillatory zoning. This evidence supports the preservation of original oxygen isotope ratios in the NPD zircons.

Radiation damage has long been recognized as possibly compromising the preservation of magmatic $\delta^{18}O$ values in zircon (see Valley, 2003). In general, alteration causes compositions to be more variable and from grain to grain, and heterogeneous within individual grains. Valley et al. (1994) first showed a correlation of $\delta^{18}O$ with U–Pb age concordance and [U] in ca. 1 Ga zircons from the Adirondack Mountains with shifts of up to 2 ‰ for poorly concordant analyses of bulk concentrates. These analyses mixed many grains together and are average values of pristine and altered domains. Clearly, *in-situ* analyses would encounter more extreme values and greater heterogeneity still.

Values of $\delta^{18}O$ in the NPD rhyolite zircon, measured *in-situ*, represent a tight range and there is no correlation to [Ca] values that range from 4 to 1632 ppm (Fig. 10a). Likewise the oxygen isotope ratios in zircon show no correlation with Hf, Th/U and other trace elements (see Supplementary Fig. S5). Furthermore, $\delta^{18}O$ does not correlate with α-dose, which was calculated from Th and U concentration and U–Pb age (Fig. 10b). These results support the conclusion that NPD zircons have retained original, magmatic oxygen isotope ratios.

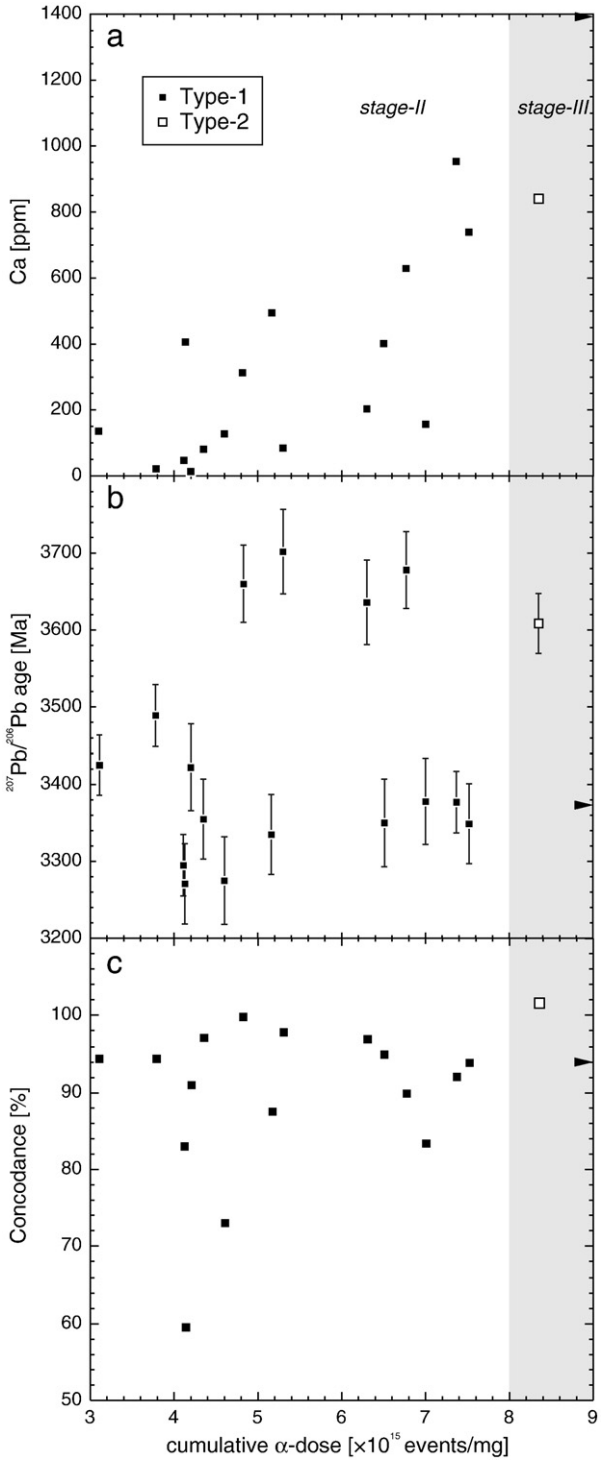

Fig. 9. Correlation of cumlative, unanneled α-dose with Ca (ppm) (a), $^{207}Pb/^{206}Pb$ age (b) and concordance (%) (c). All data are from cores of the dated NPD rhyolite zircons. Values of α-dose can be correlated to radiation damage in zircon only if there has not been annealing at ≥200 °C. Shaded area shows stage-III of radiation damage defined by α-dose calculated from [U], [Th] and age (Murakami et al., 1991). One outlier zircon plots in stage-III and off the diagram at 2.03×10^{16} events/mg. The y-axis value of the outlier spot is indicated by a solid triangle. All analyzed spots are above the first percolation point (2×10^{15} events/mg) (Ríos et al., 2000). (a) Calcium concentrations in the NPD rhyolite zircons correlate with the cumulative α-dose. The stage-III spot has the highest Ca concentration (1392 ppm). (b, c) The α-dose and concordance do not correlate with $^{207}Pb/^{206}Pb$ age (Kitajima et al., 2008). Error bars in (b) represent 2σ errors of $^{207}Pb/^{206}Pb$ age.

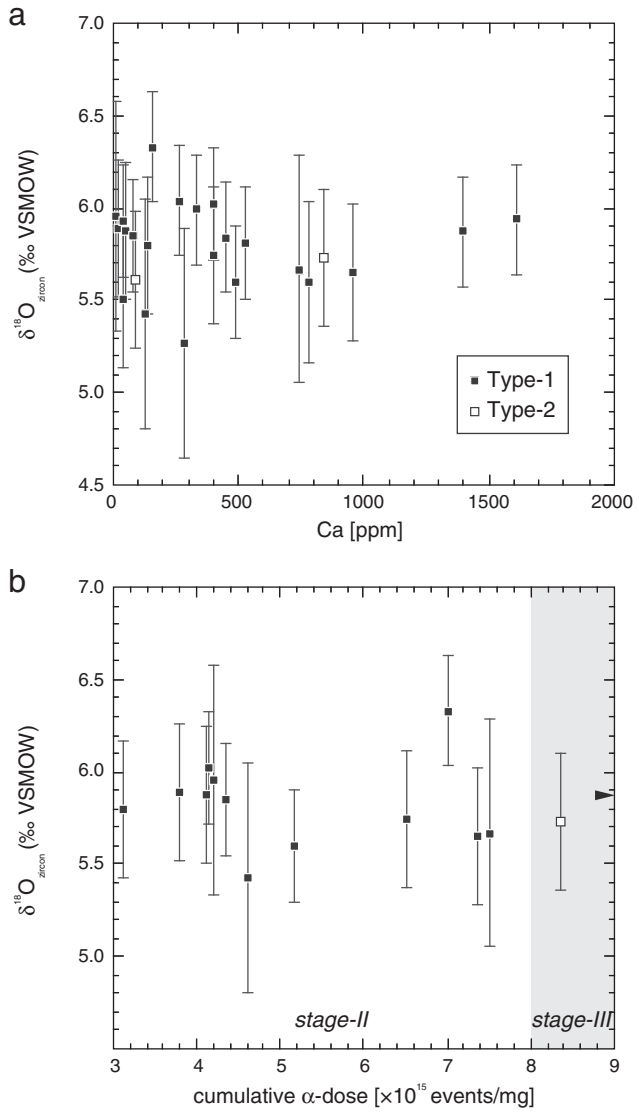

Fig. 10. Oxygen isotope ratio ($\delta^{18}O$) against Ca (a) and cumlative α-dose (b). Error bars for $\delta^{18}O$ are 2SD. Solid and open squares are Type-1 and Type-2 spots, respectively. The values of $\delta^{18}O$ in the NPD rhyolite zircon do not correlate with [Ca] or α-dose.

7. Conclusions

The oxygen isotope ratios in ~3.3–3.7 Ga Archean zircons from the Panorama Formation in Western Australia show a narrow range ($\delta^{18}O = 5.78 \pm 0.46$ ‰; 2SD, n = 48) irrespective of U–Pb age. These $\delta^{18}O$ values are similar to other Archean zircons from felsic volcanic rocks and granitoids.

Calcium and P in the NPD rhyolite zircons correlate with a 3/1 atomic ratio. SEM observations and the P/Ca ratio show that there is no contribution to SIMS analysis pits from phosphate mineral inclusions in zircon. Calcium concentration (up to 1614 ppm) also correlates with other trace elements such as Ti, Fe and ΣREE. Calcium is an index of alteration in zircons. The Ca enrichment in the NPD rhyolite zircons correlates with cumulative α-dose (calculated from [U], [Th] and $^{207}Pb/^{206}Pb$ age), suggesting that enrichment of Ca and other trace elements in the NPD rhyolite zircons was faciliated by nm-scale defects resulting from partially- to unannealed-radiation damage.

Some zircons in the NPD rhyolite are characterized by M-HREE (Dy/Dy^*) enrichment that correlates with higher [Ca] and α-dose, but not LREE enrichment. These results suggest that M–HREE enrichment in the NPD rhyolite zircon also resulted due to radiation damage. This alteration style in zircon shows the importance to monitor Ca concentration in zircon.

Despite the alteration and radiation damage, oxygen isotopes in the NPD rhyolite zircons have a tight range of magmatic $\delta^{18}O$ value that is typical of Archean igneous zircons. This shows that oxygen isotope ratios in zircon can be more robust and reliable than trace elements including REEs.

Acknowledgements

The authors thank Masaru Terabayashi, Taro Kabashima, and Yuichiro Ueno for assistance with fieldwork; Brian Hess for sample preparation; Jim Kern for profilometer analyses; John Fournelle for assistance with SEM imaging; and Reinhard Kozdon for assistance with SIMS analysis. We thank Editor Klaus Mezger, Bruce Watson and an anonymous reviewer for constructive comments. This study was partly supported by the Grant-in-Aid for JSPS Fellows (no. 19-6362) and JSPS Excellent Young Researcher Overseas Visit Program to KK. The present study was funded by NSF-EAR (0838058) and DOE (93ER14389). WiscSIMS is partially supported by NSF-EAR (0319230, 0744079, 1053466).

Appendix A. Supplementary data

Supplementary data to this article can be found online at http://dx.doi.org/10.1016/j.chemgeo.2012.09.019.

References

Bouvier, A.-S., Ushikubo, T., Kita, N., Cavosie, A., Kozdon, R., Valley, J., 2012. Li isotopes and trace elements as a petrogenetic tracer in zircon: insights from Archean TTGs and sanukitoids. Contributions to Mineralogy and Petrology 163 (5), 745–768.

Bowman, J.R., Moser, D.E., Valley, J.W., Wooden, J.L., Kita, N.T., Mazdab, F.K., 2011. Zircon U–Pb isotope, $\delta^{18}O$ and trace element response to 80 m.y. of high temperature metamorphism in the lower crust: sluggish diffusion and new records of Archean craton formation. American Journal of Science 311 (9), 719–772.

Cavosie, A.J., Valley, J.W., Wilde, S.A., E.I.M.F, 2005. Magmatic $\delta^{18}O$ in 4400–3900 Ma detrital zircons: a record of the alteration and recycling of crust in the Early Archean. Earth and Planetary Science Letters 235 (3–4), 663–681.

Cavosie, A.J., Valley, J.W., Wilde, S.A., 2006. Correlated microanalysis of zircon: Trace element, $\delta^{18}O$, and U-Th-Pb isotopic constraints on the igneous origin of complex >3900 Ma detrital grains. Geochimica et Cosmochimica Acta 70 (22), 5601–5616.

Cherniak, D.J., 2010. Diffusion in accessory minerals: zircon, titanite, apatite, monazite and xenotime. Reviews in Mineralogy and Geochemistry 72 (1), 827–869.

Claiborne, L., Miller, C., Wooden, J., 2010. Trace element composition of igneous zircon: a thermal and compositional record of the accumulation and evolution of a large silicic batholith, Spirit Mountain, Nevada. Contributions to Mineralogy and Petrology 160 (4), 511–531.

Cullers, R.L., DiMarco, M.J., Lowe, D.R., Stone, J., 1993. Geochemistry of a silicified, felsic volcaniclastic suite from the early Archaean Panorama Formation, Pilbara Block, Western Australia: an evaluation of depositional and post-depositional processes with special emphasis on the rare-earth elements. Precambrian Research 60 (1–4), 99–116.

Finch, R.J., Hanchar, J.M., Hoskin, P.W.O., Burns, P.C., 2001. Rare-earth elements in synthetic zircon: Part 2. A single-crystal X-ray study of xenotime substitution. American Mineralogist 86 (5–6), 681–689.

Fu, B., Page, F.Z., Cavosie, A.J., Fournelle, J., Kita, N.T., Lackey, J.S., Wilde, S.A., Valley, J.W., 2008. Ti-in-zircon thermometry: applications and limitations. Contributions to Mineralogy and Petrology 156 (2), 197–215.

Geisler, T., Rashwan, A.A., Rahn, M.K.W., Poller, U., Zwingmann, H., Pidgeon, R.T., Schachter, H., Tomaschek, F., 2003. Low-temperature hydrothermal alteration of natural metamict zircons from the Eastern Desert, Egypt. Mineralogical Magazine 67, 485–508.

Geisler, T., Schaltegger, U., Tomaschek, F., 2007. Re-equilibration of zircon in aqueous fluids and melts. Elements 3 (1), 43–50.

Grimes, C.B., John, B.E., Kelemen, P.B., Mazdab, F.K., Wooden, J.L., Cheadle, M.J., Hanghøj, K., Schwartz, J.J., 2007. Trace element chemistry of zircons from oceanic crust: a method for distinguishing detrital zircon provenance. Geology 35 (7), 643–646.

Grimes, C., Ushikubo, T., John, B., Valley, J., 2011. Uniformly mantle-like $\delta^{18}O$ in zircons from oceanic plagiogranites and gabbros. Contributions to Mineralogy and Petrology 161 (1), 13–33.

Hofmann, A., Valley, J., Watson, E., Cavosie, A., Eiler, J., 2009. Sub-micron scale distributions of trace elements in zircon. Contributions to Mineralogy and Petrology 158 (3), 317–335.

Hoskin, P.W.O., 2005. Trace-element composition of hydrothermal zircon and the alteration of Hadean zircon from the Jack Hills, Australia. Geochimica et Cosmochimica Acta 69 (3), 637–648.

Hoskin, P.W.O., Schaltegger, U., 2003. The composition of zircon and igneous and metamorphic petrogenesis. In: Hanchar, J.M., Hoskin, P.W.O. (Eds.), Zircon. : Reviews in Mineralogy and Geochemistry, 53. Mineralogical Society of America, Washington DC, USA, pp. 27–62.

Ireland, T., Williams, I.S., 2003. Considerations in zircon geochronology by SIMS. In: Hanchar, J.M., Hoskin, P.W.O. (Eds.), Zircon. : Reviews in Mineralogy and Geochemistry, 53. Mineralogical Society of America, Washington DC, USA, pp. 215–241.

Kita, N.T., Ushikubo, T., Fu, B., Valley, J.W., 2009. High precision SIMS oxygen isotope analysis and the effect of sample topography. Chemical Geology 264 (1–4), 43–57.

Kitajima, K., Hirata, T., Maruyama, S., Yamanashi, T., Sano, Y., Liou, J.G., 2008. U – Pb zircon geochronology using LA-ICP-MS in the North Pole Dome, Pilbara Craton, Western Australia: a new tectonic growth model for the Archean chert/greenstone succession. International Geology Review 50 (1), 1–14.

Murakami, T., Chakoumakos, B.C., Lumpkin, G.R., Weber, W.J., 1991. Alpha-decay event damage in zircon. American Mineralogist 76, 1510–1532.

Nishizawa, M., Terada, K., Ueno, Y., Sano, Y., 2004. Ion microprobe U – Pb dating and REE analysis of apatite from kerogen-rich silica dike from North Pole area, Pilbara Craton, Western Australia. Geochemical Journal 38, 243–254.

Page, F.Z., Fu, B., Kita, N.T., Fournelle, J., Spicuzza, M.J., Schulze, D.J., Viljoen, F., Basei, M.A.S., Valley, J.W., 2007a. Zircons from kimberlite: new insights from oxygen isotopes, trace elements, and Ti in zircon thermometry. Geochimica et Cosmochimica Acta 71 (15), 3887–3903.

Page, F.Z., Ushikubo, T., Kita, N.T., Riciputi, L.R., Valley, J.W., 2007b. High-precision oxygen isotope analysis of picogram samples reveals 2 μm gradients and slow diffusion in zircon. American Mineralogist 92 (10), 1772–1775.

Parrish, R.R., Noble, S.R., 2003. Zircon U – Th – Pb geochronology by isotope dilution — thermal ionization mass spectrometry (ID-TIMS). Reviews in Mineralogy and Geochemistry 53 (1), 183–213.

Rayner, N., Stern, R.A., Carr, S.D., 2005. Grain-scale variations in trace element composition of fluid-altered zircon, Acasta Gneiss Complex, northwestern Canada. Contributions to Mineralogy and Petrology 148 (6), 721–734.

Ríos, S., Salje, E.K.H., Zhang, M., Ewing, R.C., 2000. Amorphization in zircon: evidence for direct impact damage. Journal of Physics. Condensed Matter 12 (11), 2401–2412.

Sanborn, N., Stern, R., Desgreniers, S., Botton, G.A., 2000. Microstructure of neorchean zircon from the Acasta gneiss complex, northwest territories. Geological Survey of Canada, Current Research 2000-F3 (Radiogenic age and isotopic studies: Report 13). Geological Survey of Canada . 12 pp.

Smithies, R.H., Champion, D.C., Van Kranendonk, M.J., Martin, J., van Kranendonk, R.H.S., Vickie, C.B., 2007. The oldest well-preserved felsic volcanic rocks on earth: geochemical clues to the early evolution of the Pilbara Supergroup and implications for the growth of a Paleoarchean protocontinent. Dev. Precambrian Geol., Volume 15. Elsevier, pp. 339–367.

Terabayashi, M., Masuda, Y., Ozawa, H., 2003. Archean ocean-floor metamorphism in the North Pole area, Pilbara Craton, Western Australia. Precambrian Research 127, 167–180.

Thorpe, R.I., Hickman, A.H., Davis, D.W., Mortensen, J.K., Trendall, A.F., 1992. U – Pb zircon geochronology of Archaean felsic units in the Marble Bar region, Pilbara Craton, Western Australia. Precambrian Research 56, 169–189.

Ushikubo, T., Kita, N.T., Cavosie, A.J., Wilde, S.A., Rudnick, R.L., Valley, J.W., 2008. Lithium in Jack Hills zircons: evidence for extensive weathering of Earth's earliest crust. Earth and Planetary Science Letters 272 (3–4), 666–676.

Utsunomiya, S., Valley, J.W., Cavosie, A.J., Wilde, S.A., Ewing, R.C., 2007. Radiation damage and alteration of zircon from a 3.3 Ga porphyritic granite from the Jack Hills, Western Australia. Chemical Geology 236 (1–2), 92–111.

Valley, J.W., 2003. Oxygen isotopes in zircon. In: Hanchar, J.M., Hoskin, P.W.O. (Eds.), Zircon. Reviews in Mineralogy and Geochemistry., 53. Mineralogical Society of America, Washington DC, USA, pp. 343–385.

Valley, J.W., Kita, N.T., 2009. *In situ* oxygen isotope geochemistry by ion microprobe. Mineralogical Association of Canada Short Course 41, 19–63.

Valley, J.W., Chiarenzelli, J.R., McLelland, J.M., 1994. Oxygen isotope geochemistry of zircon. Earth and Planetary Science Letters 126 (4), 187–206.

Valley, J.W., Kinny, P.D., Schulze, D.J., Spicuzza, M.J., 1998. Zircon megacrysts from kimberlite: oxygen isotope variability among mantle melts. Contributions to Mineralogy and Petrology 133, 1–11.

Valley, J., Lackey, J., Cavosie, A., Clechenko, C., Spicuzza, M., Basei, M., Bindeman, I., Ferreira, V., Sial, A., King, E., Peck, W., Sinha, A., Wei, C., 2005. 4.4 billion years of crustal maturation: oxygen isotope ratios of magmatic zircon. Contributions to Mineralogy and Petrology 150 (6), 561–580.

Van Kranendonk, M.J., 2006. Volcanic degassing, hydrothermal circulation and the flourishing of early life on Earth: a review of the evidence from c. 3490–3240 Ma rocks of the Pilbara Supergroup, Pilbara Craton, Western Australia. Earth-Science Reviews 74, 197–240.

Van Kranendonk, M.J., Hickman, A.H., Williams, I.S., Nijman, W., 2001. Archaean geology of the East Pilbara Granite–Greenstone Terrane, Western Australia — a field guide, Record 2001/9. Western Australia Geological Survey . 134 pp.

Watson, E., Wark, D., Thomas, J., 2006. Crystallization thermometers for zircon and rutile. Contributions to Mineralogy and Petrology 151 (4), 413–433.